



Citation for published version:

Al Hosani, E, Zhang, M & Soleimani, M 2015, 'A limited region electrical capacitance tomography for detection of deposits in pipelines', *IEEE Sensors Journal*, vol. 15, no. 11, pp. 6089-6099.
<https://doi.org/10.1109/JSEN.2015.2453361>

DOI:

[10.1109/JSEN.2015.2453361](https://doi.org/10.1109/JSEN.2015.2453361)

Publication date:

2015

Document Version

Early version, also known as pre-print

[Link to publication](#)

© 2015 IEEE. Personal use of this material is permitted. Permission from IEEE must be obtained for all other users, including reprinting/ republishing this material for advertising or promotional purposes, creating new collective works for resale or redistribution to servers or lists, or reuse of any copyrighted components of this work in other works.

University of Bath

General rights

Copyright and moral rights for the publications made accessible in the public portal are retained by the authors and/or other copyright owners and it is a condition of accessing publications that users recognise and abide by the legal requirements associated with these rights.

Take down policy

If you believe that this document breaches copyright please contact us providing details, and we will remove access to the work immediately and investigate your claim.

A limited region electrical capacitance tomography for detection of deposits in pipelines

Esra Al Hosani , Maomao Zhang, , Manuchehr Soleimani

Engineering Tomography Laboratory (ETL), Department of Electronic and Electrical Engineering,
University of Bath, Bath, UK. m.soleimani@bath.ac.uk

ABSTRACT- Pipeline deposits are a worldwide problem facing the process industry affecting all phases of production, transmission and distribution causing problems to the pipeline operations up to the customer delivery point. Therefore, monitoring the propagation of such deposits at different points of the pipeline network will help taking more adequate preventive actions. Several good technologies are available in the market nowadays for monitoring deposits but Electrical Capacitance Tomography (ECT) technique in particular promises superior advantages as it is considered fast, compact, safe, easy to interpret and cost effective. However, ECT still suffers from one disadvantage being the poor resolution, thus this study suggest the use of ECT with limited region tomographic image reconstruction using a narrowband pass filter to enhance the resolution of the produced images. The experimental results showed that different deposits regimes and fine deposits could be detected with high definition and high resolution.

Keywords: ECT, pipeline deposits monitoring, limited region tomography

1 INTRODUCTION

Different forms of deposits continue to present in pipelines of many modern process industries especially the oil and gas sector. The type of deposits depends on the pipeline material and the composition of the transported material in the pipeline. Examples of deposits are mineral scales [1], paraffin (wax) [2-3] and black powder [4-5].

Scale is the accumulation of deposits that coat the interior of pipelines and other production facilities such as casing, perforation valves and pumps. Black Powder is a general term for contaminants in gas pipelines; it is comprised of numerous forms of iron sulfide, iron oxide and iron carbonate. Sometimes these main components are mixed with other contaminants in the gas pipeline such as rouge, asphaltenes, sand, liquid hydrocarbons, metal debris and/or salt. The combinations of these contaminants appear in black dry powder, liquid or sludge suspension, depending on pipeline conditions; however the term “powder” is general.

Black powder consists of sub-micron sized particles making it easy to transport inside pipeline system causing problems not only in pipeline operations but also at the customer delivery point such as fouling of compressors, contamination of instrumentation and control valves or even plugging filter systems. On the other hand scale and wax formation over time can cause pipeline failures with critical consequences such as serious environmental impact, safety concerns, and added costs for clean up, maintenance and unscheduled production shutdown. Also,

it can cause pressure drop that lowers the flow rate by building up on the inner pipeline walls forming a flow restriction, this requires additional horsepower to achieve the same flow rates which is an additional operating expense.

A subsurface image of the pipe will surely help assessing the condition of the pipe in terms of deposits, and therefore help to monitor and possibly automate the process for both quality assurance and field inspections, thus increasing productivity, efficiency and safety. However, in order to achieve this goal, the imaging technique should be non-destructive, non-intrusive, cost efficient, accurate and safe. There are various techniques available for process tomography for imaging the subsurface properties of materials. A comprehensive review of the different process tomography techniques was conducted by [6], and a specific review of all state of the art inspection technologies for condition assessment of pipelines were given by [7-9]. However, not all techniques are applicable for deposit detection, especially hydrocarbon deposits, which often present in oil refineries or polymer producing plants [10]. Thus, in the process industry, most commercial technologies such as radiographic, ultrasonic or electromagnetic are used for pipe inspection purposes where pits, cracks and damages in metallic pipelines are the primary concern.

Today, in the oil and gas industry in particular, operators use three techniques to avoid blockage caused by deposits, 1- chemical injection in the pipeline flow, which is a costly method, 2- periodic pigging of the pipeline, which disturbs the production and/or 3- separation techniques (e.g. filtering and cyclones), which disturbs the flow. However, instead of waiting for a problem to occur, detecting the formation of deposits in the early stages will help preventing many of the discussed problems. The monitoring can be done in critical places where deposits are more likely to exist or/and before customer delivery point as a quality assurance procedure. Continuous monitoring methods for pipelines are in the stage of research and this paper in one step further to provide a solution to this problem.

Table 1 gives a comparison between the most popular imaging techniques used for inspecting pipelines non-destructively for deposits, namely visual inspection, ultrasonic, radiography and infrared thermography. Table 1 summarizes the principle of operation of each technique, their commercial availability, their advantages and disadvantages. All of the compared techniques in table 1 share the advantage of being non-invasive and non-intrusive. However, their individual advantages should be weighed carefully against their disadvantages before choosing the proper technique for a particular application. For instance, some of the eminent techniques used in the process industry for non-destructive testing such as ultrasonic, radiography and thermography techniques are mostly suitable for metallic pipes. Although some promising research work was conducted in different companies and universities laboratories to try to adapt them for poly or/and concrete pipes [11], these techniques are still commercially available for metallic pipes only. Also most of the techniques are relatively slow and requires a trained operator to set up the test and interpret the results properly.

On the other hand, ECT technique offers the combined advantage of being fast, compact, safe, easy to interpret and cost effective. Thus, ECT is considered in this paper to image the internal cross section of a poly pipe to detect the formation of deposits. Poly pipes are

superseding their metallic and concrete counterparts and are being more popular in industries such as oil, gas and water due to their advantages of being resistant to chemical processes, cost effective, light and easy to install [12]. However ECT has the prominent drawback of offering low-resolution images due to the ill-posedness, ill-conditioning and non-linearity of the ECT problem. Therefore, this paper aims to present a new enhanced technique based on limited region tomographic image reconstruction for ECT to detect deposits in poly pipes.

In this paper, section 2 introduces the ECT system, section 3 describes the image reconstruction method used and developed while section 4 shows the experimental results from the laboratory experiments. Section 5 gives an analysis of the results and explains why the particular limited region imaging works better for deposit inspection.

Table 1 Common non-destructive imaging techniques used for inspecting deposits in pipelines.

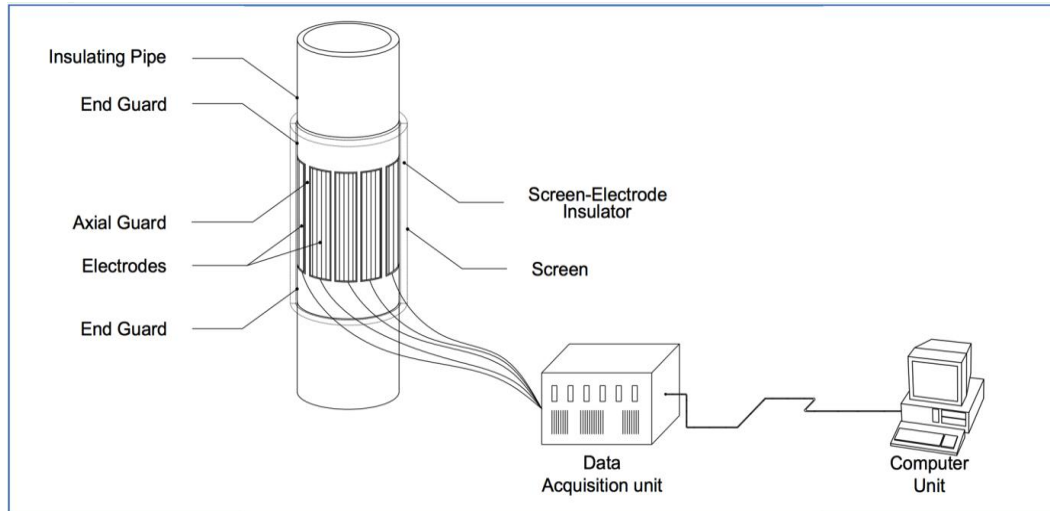
Imaging method	Principle of operation	Commercial availability	Advantages	Disadvantages
Visual inspection	A CCTV camera and lighting device (or laser) attached on a mechanical or electronic carrier.	Different types are commercially available for research and process applications i.e pan and tilt and Side scanning evaluation technology (SSET).	<ul style="list-style-type: none"> • High definition video of the inspection can be achieved. • The survey can be done online or off-line. • The operator has full control of the inspection (pan, tilt or zoom the camera) • Easy interpretation of the images. 	<ul style="list-style-type: none"> • The speed of the carrier is relatively slow (15-30 cm/s) to capture an analysable video. • The carrier must stop at multiple adjacent locations for inspection. • Only large pipes that can accommodate the carrier and the camera can be inspected. • The inspection requires the process to be stopped and the pipe to be emptied.
Ultrasonic [13]	High frequency sound waves are applied at the exterior of the pipe. The sound waves will travel through the pipe and then reflect back to their source when encountering a boundary with another medium (any fluid inside the pipe). The reflected sound waves are used to determine the thickness of the pipe.	Different types are commercially available for research and process applications i.e contact technique (requires a couplant) and Non-contact techniques (Laser and Electro Magnetic Acoustic Transducers (EMAT) [14]).	<ul style="list-style-type: none"> • Good resolution. • Access to only one side of the pipe is required when the pulse-echo technique is used. • Deep penetration into the pipe, which permits detecting deep flaws and deposits. • High sensitivity, which allows the detection of small deposits and flaws. • Can cover high range of the inspected pipe. • No need to shut down the pipeline for the inspection. 	<ul style="list-style-type: none"> • Requires a trained operator in order to set up the test and interpret the results properly. • Complex pipe geometries are more challenging to inspect. • Calibration with respect to the pipe material is required prior to the inspection. • Generally requires contact medium (couplant).
Radiography	A source of radiation emits photons/neutrons through the pipe and onto a photographic film or a digital camera that record the absorbed radiation, which is used to reconstruct an image.	Different types are commercially available for research and process applications i.e Gamma rays X-rays.	<ul style="list-style-type: none"> • High resolution images can be achieved • Ability to inspect complex pipe geometries. • High sensitivity to changes in the pipe density. 	<ul style="list-style-type: none"> • Potential health hazards associated with the inspection. • Relatively expensive. • Relatively slow. • Sensitive to the flaw orientation.
Infrared Thermography	According to the black body radiation law, all objects above absolute zero kelvin emit thermal infrared radiation.	Different types are commercially available for research and process	<ul style="list-style-type: none"> • Non-contact technique. • Easy interpretation of the images (given that they are accurate) • Large areas can be 	<ul style="list-style-type: none"> • Relatively expensive. • In active thermography, the pipe is heated first before inspection, which makes the process slower. • The operating condition that

	Consequently, thermographic cameras are used to detect radiation in the thermal infrared range of the electromagnetic spectrum (900–14,000 nm) and produce corresponding images. Since the amount of radiation emitted by an object increases with temperature (warm bodies stand out against cooler backgrounds), an external heat source is usually used to heat the inspected pipe (active thermography).	applications i.e pulse thermography, lock-in thermography, stepped heating thermography, and vibro-thermography.	scanned at once.	must be considered is somewhat drastic i.e wind speed, cloud cover, solar radiation, dust etc. <ul style="list-style-type: none"> •Tricky to interpret since it is only able to detect direct surface temperature and from external images the interior of a pipe can be predicted [15] (i.e wall loss caused by corrosion will emit more heat) •Performing thermographic inspections does not require a certified or licensed operator, however, a trained operator is essential to operate the device and interpret the results. •Accuracy depends on several factors i.e emissivity value, compensation of the reflected temperature, ambient temperature, distance, angle of view etc. •Not efficient for concrete and poly pipes [7,10].
--	--------------------------------------------------------------------------------------------------------------------------------------------------------------------------------------------------------------------------------------------------------------------------------------------------------------------------------------------------------------------------------------------------------------	------------------------------------------------------------------------------------------------------------------	------------------	-----------------------------------------------------------------------------------------------------------------------------------------------------------------------------------------------------------------------------------------------------------------------------------------------------------------------------------------------------------------------------------------------------------------------------------------------------------------------------------------------------------------------------------------------------------------------------------------------------------------------------------------------------------------------------------------------------------------------------------------------------------------------------------------

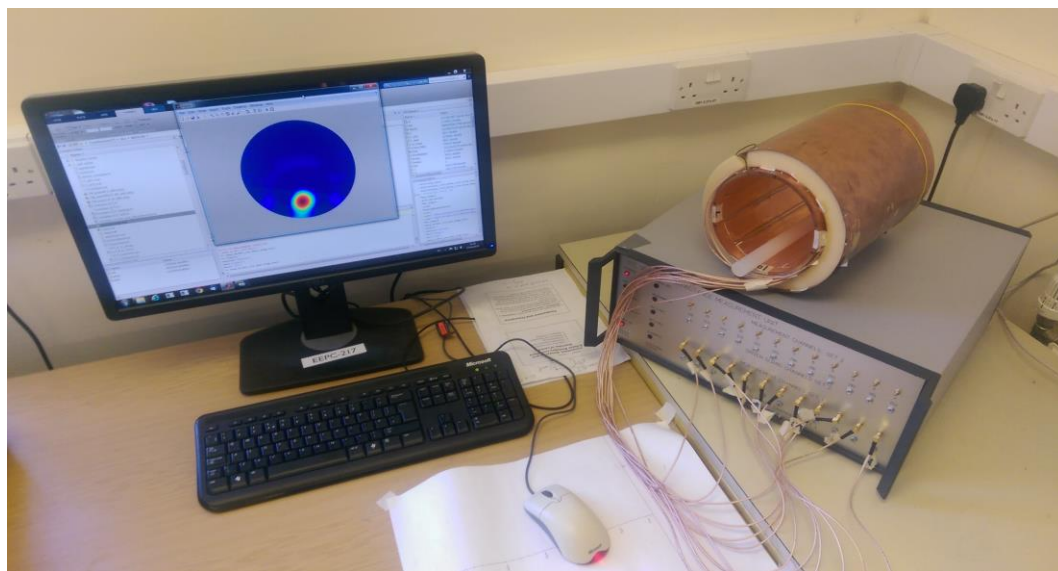
2 ECT SYSTEM

Electrical capacitance tomography is one method of process tomography used in industrial process monitoring for imaging cross-sections of a pipe/vessel. It measures the external capacitance of the enclosed objects to determine the internal permittivity distribution, which is then used to reconstruct an image of the process. Electrical Capacitance Tomography (ECT) was first developed in the late 1980's to image a two-phase flow [16]. Afterwards, ECT systems were used successfully in numerous research investigations for industrial multi-phase processes including gas/solid distribution in pneumatic conveyors [17], fluidized beds [18-20], flame combustion [21-23], gas/liquid flows [24], water/oil/gas separation process [25], water hammer [26], determining the characteristic of the molten metal in Lost Foam Casting process [27], and many others. This paper presents a new application area for ECT as a novel detection tool for deposits and scale formation in pipelines.

A distribution of different materials with different permittivity inside a pipe or a vessel leads to a random distribution of their permittivity. By measuring the capacitance of the media in a specific region, the permittivity distribution can be found, which then is used to reconstruct an image representing the same region. Mainly, ECT systems are used to image a non-conductive media. However, some conducting medias, such as water, are being recently investigated with different conditions. Fig. 1 illustrates a typical ECT system, which consists mainly of three subsystems; the capacitance sensor, data acquisition unit and computer unit.



(a)



(b)

Fig. 1. The ECT Sensor array and system (a) schematic of the ECT system (b) ECT system in the University of Bath Engineering Tomography Lab

The capacitance sensor consists of electrodes, an external shield, an axial, and a radial guards. Typically, several electrodes are mounted equidistantly on the periphery of a non-conductive process pipe or vessel. Only non-conductive pipes can be imaged non-invasively. The **neighbouring** electrodes are separated from each other by a **small slice of copper called** the axial guard. The electrodes are covered by a screen (conductive) to reduce external electrical noise, eliminate the effects of external grounded objects and protect the electrodes from damages. In case of conductive pipelines (i.e metallic), the sensor can be instead mounted internally, using the conductive internal wall of the pipeline as a screen. Alternatively, the sensor with an insulating pipe can be installed inline with the process. An insulating material must fill the gap between the

electrodes and the screen. The sensor also includes radial guards in order to reduce the standard capacitance between adjoining electrode pairs. Numerous combinations of different configurations of the radial and axial guards were suggested to improve the system performance. The screen and the radial guards are always maintained at earth potential. Fig. 3 illustrates a cross-sectional view of the typical 12-electrode ECT sensor. Other shapes of ECT sensors have been used, however, circular sensors are the most common.

For an N electrode system, various measurement protocols can be used. However, in a typical ECT system, electrodes 1 to N are used successively as source electrodes, and the capacitance values between all single electrodes combinations are measured. Hence, for one measurement cycle, electrode 1 is first excited with a fixed positive voltage making it the source electrode while electrode 2 to 12 are held at earth potential (zero) by 11 capacitance transducers making them the receiving electrodes. Then the capacitances between 1-2, 1-3, ..., 1-12 are measured simultaneously using the transducers. Next, electrode 2 is selected as the source electrode and electrodes 3 to 12 as the detecting electrodes, while electrode 1 is connected to earth making it inactive because of reciprocity (measurement 2-1 is same as 1-2). This process continues until, electrode 11 is selected as the source electrode and electrode 12 as the detecting electrode, while electrodes 1 to 10 are held inactive. Generally, the number of independent capacitance measurements is the number of N-electrode combinations, taking 2 at a time as:

$$M = \frac{N(N-1)}{2} \quad (1)$$

In an ECT system, the electrodes must be sufficiently large to provide a measureable change in capacitance. This is considered a challenge in this type of tomography, since only few electrodes can be used (usually 8 or 12), which results in limited independent measurements. This makes the image reconstruction process more challenging to produce high-resolution images.

The capacitance measurement unit plays a very important role in measuring and conditioning the signals that are achieved from the capacitance sensor (Fig. 1). This forms a main part of the ECT system (block diagram of Fig. 2). The capacitance measuring bridge is an alternating current AC bridge, which is used for measuring the inter-electrode capacitances of the sensor. Shielded SMB cables are used to connect the sensor and measurement unit. The data acquisition unit works according to the following sequence events:

1. Apply a fixed voltage, V_c , to the source electrode to excite it while keeping the rest of the detecting electrode at zero potential.
2. Measure the induced current in the receiving electrodes, and capacitive component by use of phase sensitive detector.
3. Deduce the capacitance measurement values C from the given potential difference V_c and the measured current (charge) Q according to $C = \frac{Q}{V}$.
4. Convert the capacitance measurement values into voltage signals using a type of capacitance to voltage converter,
5. Condition (amplify, filter, multiplex...etc.) and digitalize the voltage signals

6. Send the conditioned and digitalized voltage signals to a computer for processing and display.

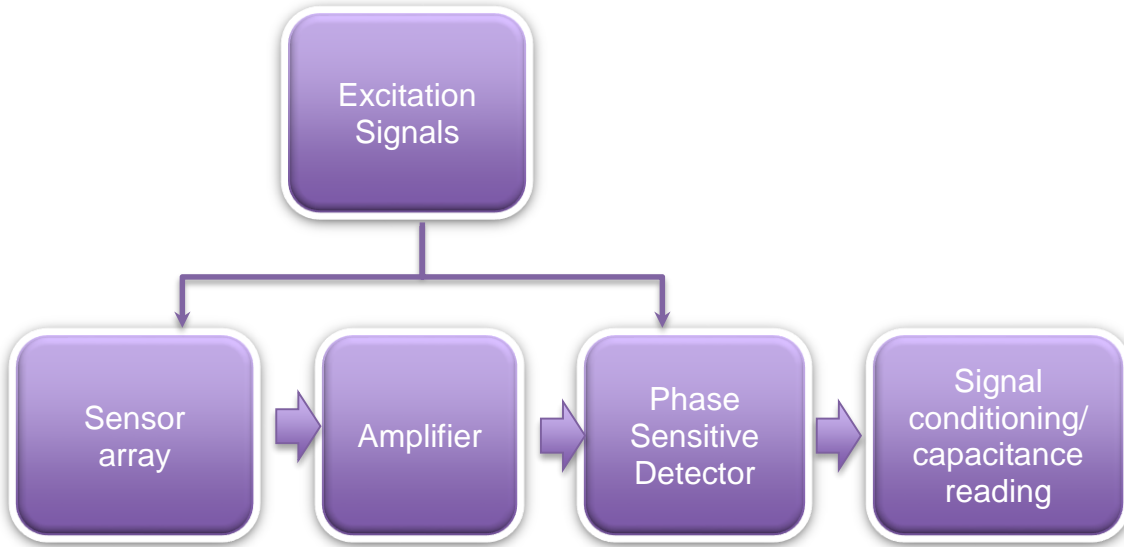


Fig. 2. A schematic drawing of the capacitive measurement unit as part of ECT data acquisition system

The received voltage signals (from the data acquisition unit) are interpreted into capacitance measurements in the computer unit in order to use them in the image reconstruction algorithm to deduce the permittivity distribution (image). The measured capacitance values C between a source electrode i and a receiving electrode j can be represented in a matrix as:

$$C_{ij} = \begin{bmatrix} C_{1,2} & C_{1,3} & \dots & C_{1,N} \\ & C_{2,3} & \dots & C_{2,N} \\ & & \ddots & \vdots \\ & & & C_{N-1,N} \end{bmatrix} \quad \text{for } \begin{matrix} i = 1, \dots, N-1 \\ j = i+1, \dots, N \end{matrix} \quad (2)$$

Although, ECT technology is still at the stage of laboratory research, it is being rapidly developing in both the hardware design and the image reconstruction quality. This is because the promising advantages of such technologies in the process industries.

3 IMAGE RECONSTRUCTION

3.1 The Forward Problem

In order to solve the inverse ECT problem, the ECT forward problem needs to be solved. The ECT mathematical system model can be treated as an electrostatic field problem and hence

can be modelled by Poisson's equation. Assuming no free charges within the field, Poisson's equation can be simplified to Laplace's equation:

$$\nabla \cdot (\varepsilon_o \varepsilon (\mathbf{x}, \mathbf{y}) \nabla \phi(\mathbf{x}, \mathbf{y})) = 0 \quad (3)$$

where ε_o is the free space permittivity, $\varepsilon (\mathbf{x}, \mathbf{y})$ and $\phi(\mathbf{x}, \mathbf{y})$ are the 2D permittivity distribution and the electrical potential distributions respectively. Laplace's equation is solved with the following Dirichlet boundary conditions:

$$\phi^i = \begin{cases} V_c & \forall (\mathbf{x}, \mathbf{y}) \subseteq \Gamma_i \quad \text{where } (i = 1, \dots, N - 1) \\ 0 & \forall (\mathbf{x}, \mathbf{y}) \subseteq \Gamma_k (k \neq i), \Gamma_{guards} \text{ and } \Gamma_{screen} \end{cases} \quad (4)$$

where V_c is a fixed voltage applied to the source electrode (electrode $i=1, \dots, 11$ one at a time), Γ_i is the spatial location of electrode i , Γ_{guards} and Γ_{screen} are the spatial location of the guards and screen respectively. On other words, equation (4) basically states that the boundary condition is some fixed voltage, V_c , applied for the source electrode and zero for the sensing electrodes, guards and screen. To further relate the permittivity distribution to the capacitance, we use the fact that the electric field is given by:

$$\mathbf{E} = -\nabla \phi(\mathbf{x}, \mathbf{y}) \quad (5)$$

also by applying Gauss law, the charge sensed by the detecting electrode j when the source electrode i is fired can be found by:

$$Q_{ij} = \int_{\Gamma_j} \varepsilon_o \varepsilon (\mathbf{x}, \mathbf{y}) \mathbf{E} \cdot \hat{\mathbf{n}} d\Gamma_j \quad \text{for } \begin{pmatrix} i = 1, \dots, N - 1 \\ j = i + 1, \dots, N \end{pmatrix} \quad (6)$$

where Γ_j is the surface of the receiving electrode and $\hat{\mathbf{n}}$ is a unit vector normal to Γ_j . Hence, the capacitance of the electrode pairs $i - j$ (inter electrode capacitances) can be calculated by:

$$C_{ij} = \frac{Q_{ij}}{V_{ij}} \quad \text{for } \begin{pmatrix} i = 1, \dots, N - 1 \\ j = i + 1, \dots, N \end{pmatrix} \quad (7)$$

where V_{ij} is the voltage difference between detector electrode and the source electrode i ($V_i - V_j$). As it can be noticed from equation (5) to (7), the measured capacitance can be linked to the permittivity distribution as:

$$C_{ij} = -\frac{\varepsilon_o}{V_{ij}} \int_{\Gamma_j} \varepsilon (\mathbf{x}, \mathbf{y}) \nabla \phi^q(\mathbf{x}, \mathbf{y}) \cdot \hat{\mathbf{n}} d\Gamma_j \quad \text{for } \begin{pmatrix} i = 1, \dots, N - 1 \\ j = i + 1, \dots, N \end{pmatrix} \quad (8)$$

where ϕ^q is the electrical potential distribution of node q in the measuring electrodes. The finite element method (FEM) is used to calculate the capacitance and the sensitivity distribution (the Jacobian matrix).

3.2 The Inverse Problem

In linearization, the change in capacitance measurements for small changes of permittivity can be approximated in a linear manner. Linearization assumes that the permittivity inside each pixel is constant because of the small size of pixels. The linearization of a nonlinear function is the first order term of its Taylor expansion near the point of interest. Therefore, the linearized system can be written as

$$\begin{aligned} \mathbf{C} &\approx \mathbf{F}(\boldsymbol{\varepsilon}_b) + \nabla\mathbf{F}(\boldsymbol{\varepsilon}_b)(\boldsymbol{\varepsilon} - \boldsymbol{\varepsilon}_b) && \text{(9 a)} \\ \text{taking } \Delta\mathbf{C} &= \mathbf{C} - \mathbf{F}(\boldsymbol{\varepsilon}_b) && \text{(9 b)} \\ \Delta\boldsymbol{\varepsilon} &= (\boldsymbol{\varepsilon} - \boldsymbol{\varepsilon}_b) && \text{(9 c)} \\ \text{and } \mathbf{s} &= \nabla\mathbf{F}(\boldsymbol{\varepsilon}_b) && \text{(9 d)} \end{aligned}$$

equations (9 a-d) can be expressed as

$$\Delta\mathbf{C} = \mathbf{s}\Delta\boldsymbol{\varepsilon} \quad \text{(9 e)}$$

Equation (9 e) represents the change in capacitance $\Delta\mathbf{C}$ in response to a change in permittivity $\Delta\boldsymbol{\varepsilon}$, where $\boldsymbol{\varepsilon}_b$ is the point of interest, and \mathbf{s} is the Frechet derivative, which represents the sensitivity of the capacitance in response to the permittivity distribution (the Jacobian). There are M equations of the form of equation (9 e) corresponding to M measurements.

The sensitivity matrix, capacitance and permittivity were normalized before processing the data in an image reconstruction algorithm so it can be used universally for different pipes with different scales. This was done to reduce systematic errors and produce better outcome. The normalized capacitance $\lambda_{i,j}$ for each capacitance measurement and the normalized permittivity g_p are given by:

$$\lambda_{i,j} = \frac{C_{i,j} - C_{i,j}^{(low)}}{C_{i,j}^{(high)} - C_{i,j}^{(low)}} \quad \text{(10)}$$

$$g_p = \frac{\varepsilon_p - \varepsilon^{(low)}}{\varepsilon^{(high)} - \varepsilon^{(low)}} \quad \text{(11)}$$

where $C_{i,j}$ is the absolute capacitance measurement and $C_{i,j}^{(high)}$ and $C_{i,j}^{(low)}$ are the absolute capacitances when the pipe is full with high permittivity (target to be imaged) and low permittivity (empty) respectively. ε_p is the absolute permittivity for pixel p , and $\varepsilon^{(high)}$ and $\varepsilon^{(low)}$ are the absolute permittivity of the target to be imaged and an empty pipe respectively. The normalized form of equation (9 e) is given by

$$\boldsymbol{\lambda} = \mathbf{S}\mathbf{g} \quad \text{(12)}$$

where $\Delta\boldsymbol{\lambda}$ is a $M \times 1$ vector, $\Delta\mathbf{g}$ is a $P \times 1$ vector and \mathbf{S} is a $M \times P$ matrix which represents the discretized sensitivity distribution of \mathbf{M} electrode pairs.

Where $\boldsymbol{\lambda}$ is the normalized capacitance vector, \mathbf{S} is the sensitivity distribution matrix of the normalized capacitances with respect to normalized permittivity distribution, and \mathbf{g} is the

normalized permittivity vector, \mathbf{g} represents the image which can be constructed by an image reconstruction algorithm.

3.3 Limited Region Tomography (LRT)

Numerous inversion algorithms were suggested for ECT image reconstruction [28-47]. However, due to the Ill-posedness, Ill-conditioning and Non-linearity of the ECT problem, the quality of the reconstructed images is still under research for enhancement. In this study, the Levenberg–Marquardt method was employed to reconstruct the permittivity distribution. First, to find the initial image, standard Tikhonov regularization is used for minimizing the objective functional:

$$\mathbf{arg\,min}_g J(\mathbf{g}) = \|\mathbf{S}\mathbf{g} - \boldsymbol{\lambda}\|_2^2 + \alpha\|L_k(\mathbf{g} - \bar{\mathbf{g}})\|_2^2 \quad (13)$$

where $\alpha > 0$ is the regularization parameter, L_k is a finite difference operator with $k \geq 0$ and $\bar{\mathbf{g}}$ is the estimated solution based on a priori information. By solving the optimization equation (13) for $\bar{\mathbf{g}} = \mathbf{0}$ and $k=0$ (giving $L_0 = I$, where I is the identity matrix), an explicit solution, denoted by $\hat{\mathbf{g}}$, is obtained:

$$\hat{\mathbf{g}} = (\mathbf{S}^T\mathbf{S} + \alpha I)^{-1}\mathbf{S}^T\boldsymbol{\lambda} \quad (14)$$

The Levenberg–Marquardt method was successfully applied to ECT before; however, this paper suggests a modification to the method taking into account prior knowledge regarding the geometry of the pipe to produce a high definition image. The proposed method is based on a limited region tomographic image reconstruction using a narrowband pass filter [48-49]. Fig 3.a shows the narrowband pass filter applied to a test pipe for deposits and scale detection. Only the “limited region” within the inner surface of the pipeline will be reconstructed to monitor the deposits and scaling condition of the pipe. The limited region is selected to be larger than the test pipe inner radius (R1) so that it can tolerate a small displacement error of the pipe from its center. This narrowband region has a relatively uniform sensitivity due to the circular cross-section of the pipe and the equal distances from ECT electrodes. This fact makes the limited region better conditioned compared to the traditional Full Region Tomography (FRT) where the sensitivity varies moderately throughout the imaging region (sensitivity increases closer to the electrodes and reduces towards the center). This particular limited region is a favourable one, making it well suited for pipe detection. The principle of the LRT is to increase the accuracy by limiting the imaging area, which consequently reduces the number of unknown pixels and thus enhance the resolution as shown in Fig. 3.b, where the region of interest (ROI) is now a fraction of the whole region. Other than the better accuracy, another advantage of the LRT over FRT is the faster performance due to the reduction of pixels used in the reconstruction. Also, because of the reduced number of pixels, the inverse problem becomes better posed in the LRT, and so is considered more robust than the FRT.

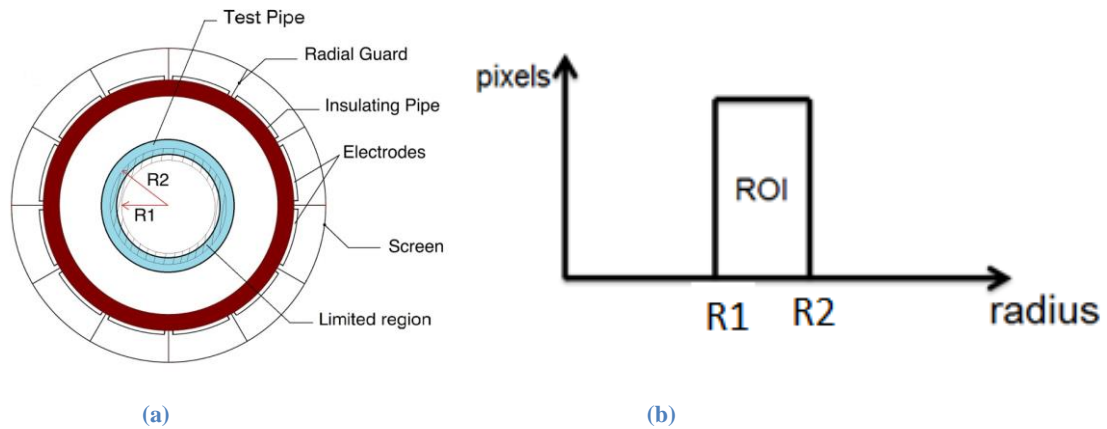


Fig. 3. Limited Region Imaging Technique for deposit detection, (a) pipe cross section view, (b) spatial narrowband pass filter

The FEM mesh model are also used for the inverse problems, 1367 and 12184 three-noded nonhomogeneous triangular elements corresponding to 739 and 6219 nodes were generated to create the mesh for the FRT and LRT respectively. However, only 691 elements of the dense LRT mesh were used to construct the limited region ring as shown in Fig. 4.

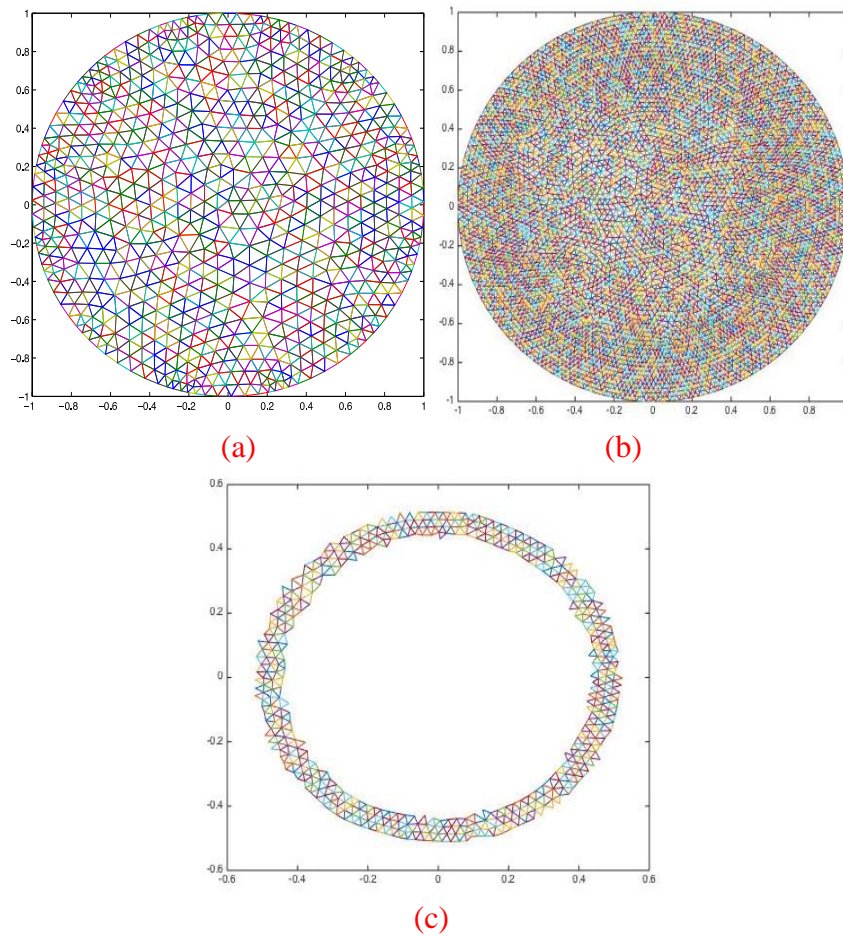


Fig. 4. FEM mesh for a) FRT b) LRT dense mesh c) Limited region ring used for the LRT

4 EXPERIMENTAL EVALUATION OF PIPELINE INSPECTION

The 12-electrode sensor used in the experiments is built in the University of Bath Engineering Tomography Lab (ETL) and has an inner diameter of 151mm (Fig. 1.b). Whilst the data acquisition unit used is a commercial PTL300E-TP-G Capacitance Measurement Unit from Process Tomography Limited, Fig. 5.a. The unit can collect sets of capacitance data at 100 frames per second with an effective resolution of 0.1 fF and measurement noise level better than 0.07 fF. Typically, sample concentrations down to 1% of the upper calibration value (corresponding to the case where the sensor is filled with the higher permittivity material) can be measured. MATLAB is used for data collection, image reconstruction and processing. Two experimental models mimicking the pipeline and pipeline deposits were prepared in the laboratory in order to simulate scale/wax and black powder deposits in real processes. The test pipe is made of polyethylene, which has a relative permittivity of 2.25. The inner and external diameter of the test pipe are 77 mm and 88mm respectively (Fig. 5.b) and it was placed in the center of the ECT sensor as shown in Fig. 3. This is because the sensitivity of the measurements in the middle of the imaging region is almost uniform.

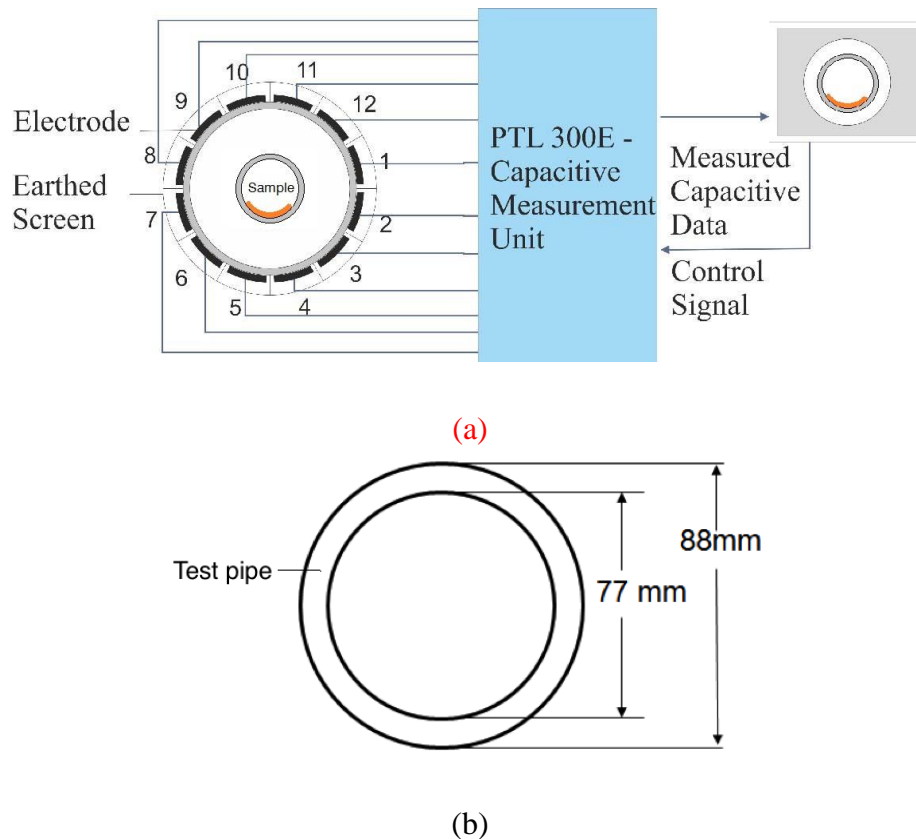


Fig. 5. (a) Block diagram of the ECT system,(b)the dimensions of the test pipe sample used for testing deposit detection

4.1 Scale and Wax Detection

To simulate the scale and wax formation inside the pipe, typical printer papers with relative permittivity of 3.85 (Fig. 6) were used to investigate 4 different cases.

- In case 1: a pile of 24 pieces of paper, which are 52.5mm wide and 297mm long, were placed internally in one side of the test pipe.
- In case 2: the two piles of paper used in case 1 were placed internally in two opposite sides of the test pipe.
- In case 3: 20 papers of a typical A4 size (210mm X 297mm) were piled and rolled inside the inner surface of the test tube.
- In case 4: case 1 and 3 were combined by adding the pile of paper used in case 1 to the setting of case 3.

For the sake of comparison, both LRT and FRT **were constructed for all cases and are** shown in Fig. 7 along with the **LRT** image after threshold processing. The threshold images are all set to 97% of the mean values of reconstructed permittivity in limited region.

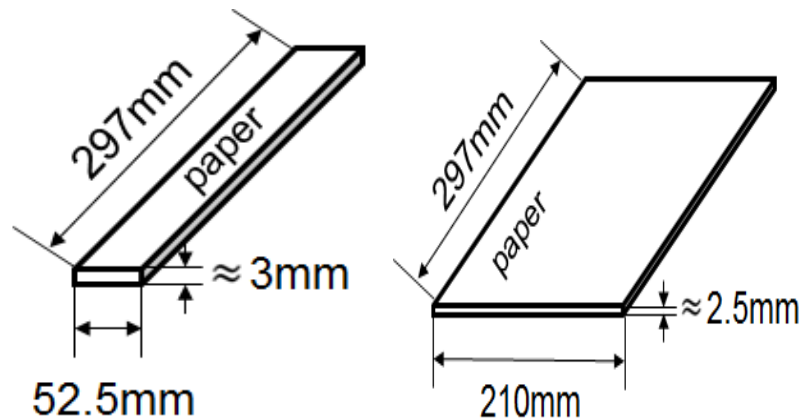
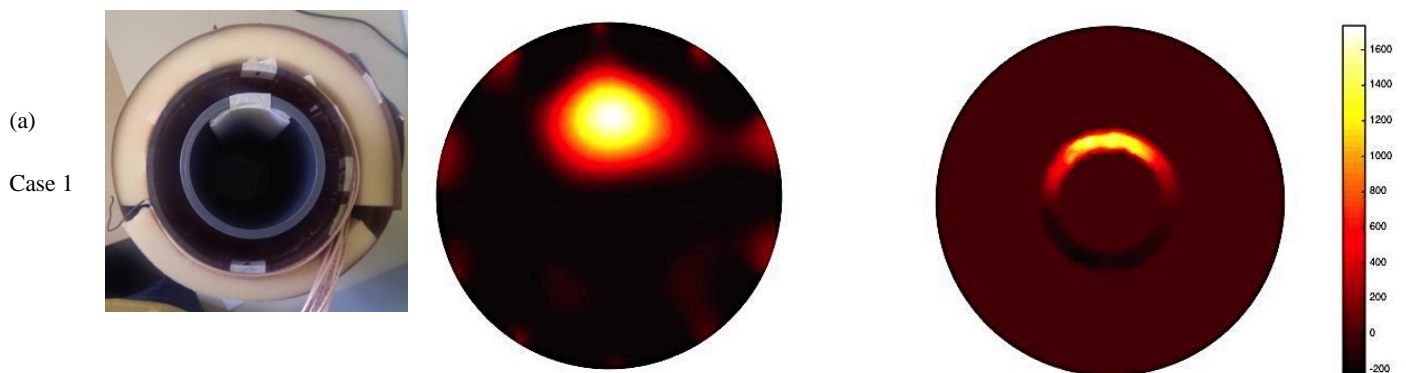


Fig. 6. The paper-folds with their dimensions



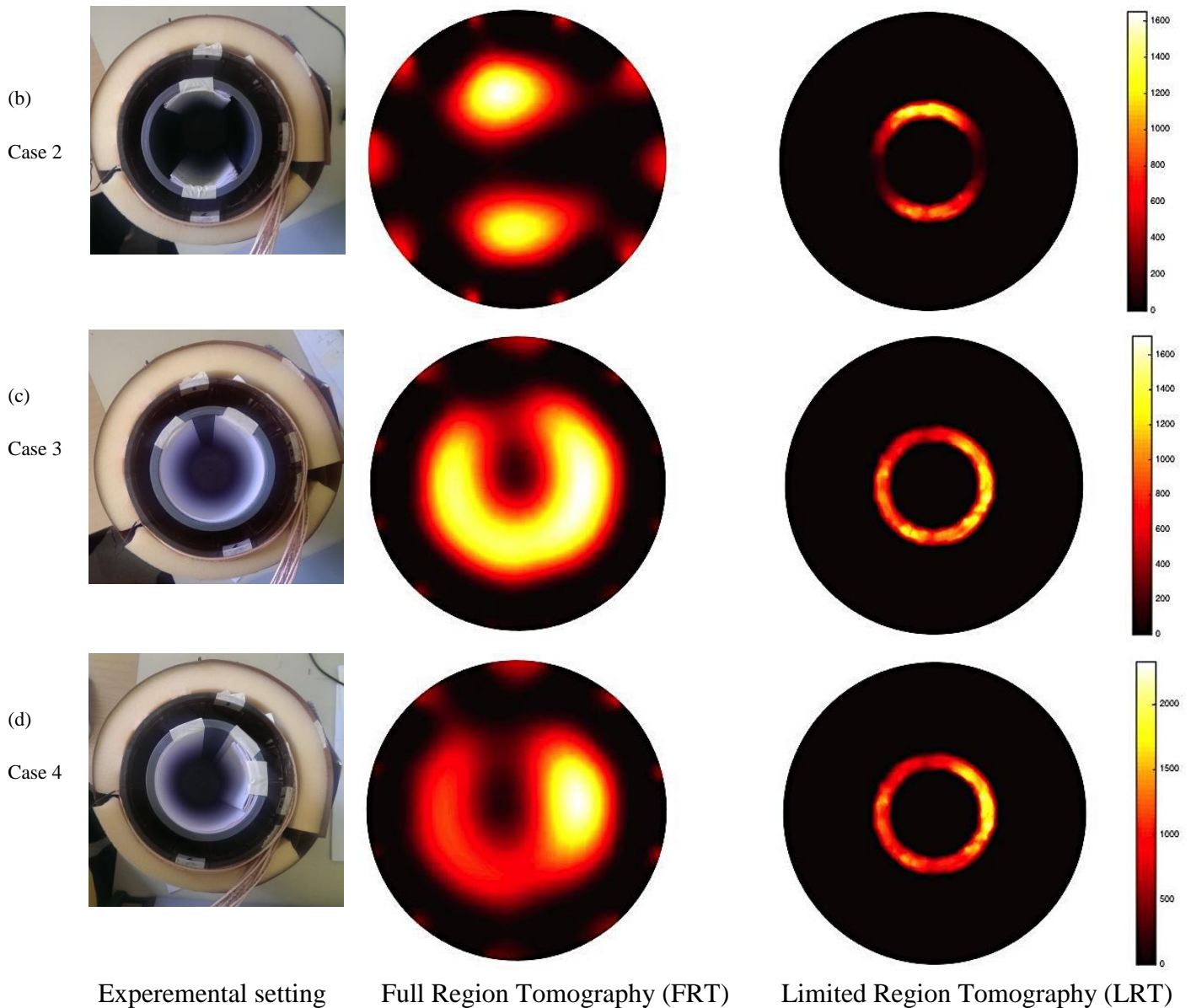
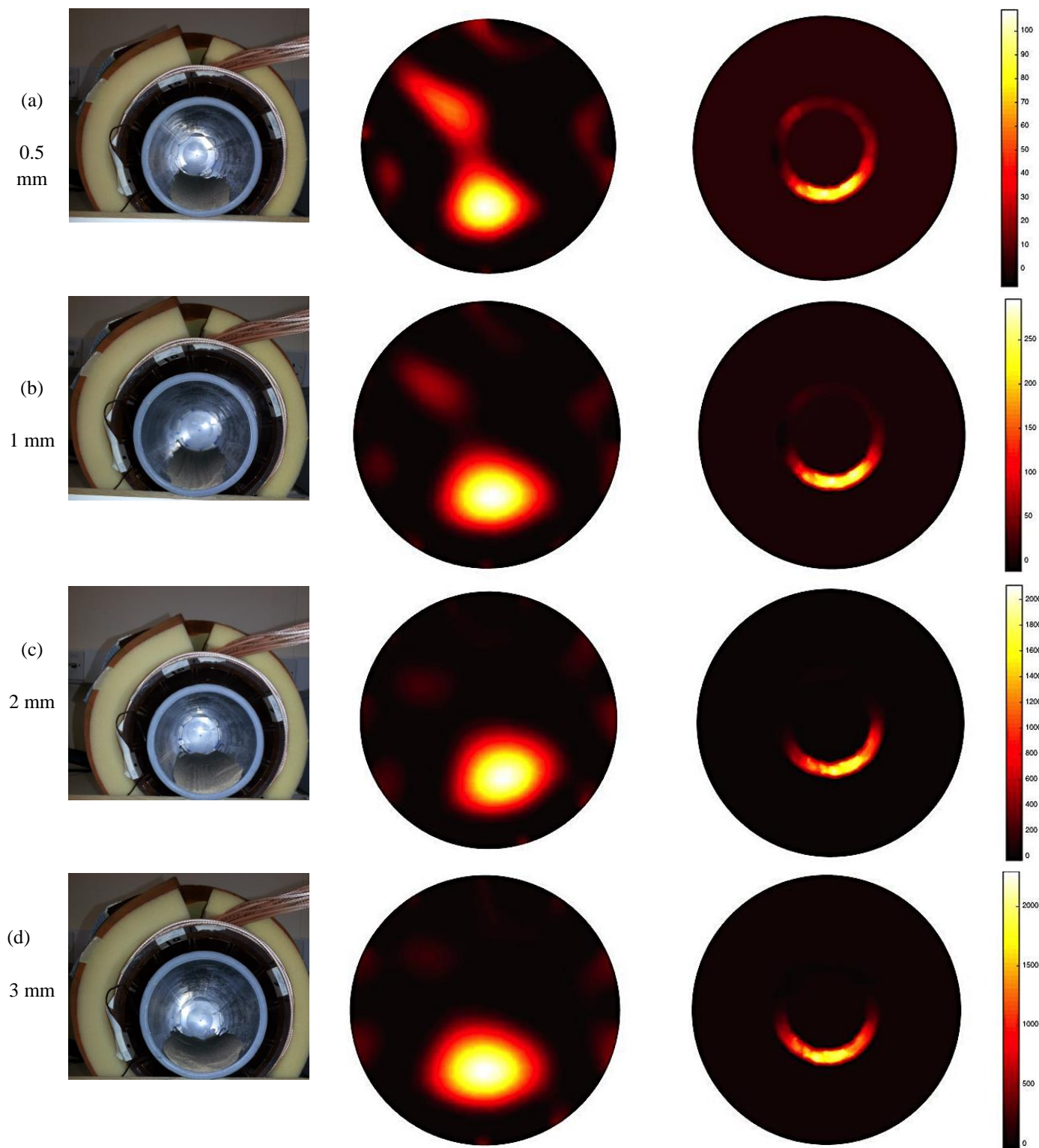


Fig. 7. Reconstruction of paper samples as models of scale and wax deposits (a) case 1, (b) case 2, (c) case 3 and (d) case 4

4.2 Black Powder Detection

In an attempt to simulate black powder deposits in pipelines, very fine sand (0.0625 – 0.125 mm diameter) with relative permittivity of 2.5-3.5 was used. Six Different layers of sand with varying thicknesses, namely, 0.5, 1, 2, 3, 4 and 5 mm were investigated and shown in Fig. 8. As it can be seen in Fig. 8 all location of deposit has been identified in both sets of images from LRT and FRT, the LRT provides superior results in identifying level of deposit. We decided not to show the thresholded images of deposit in LRT as it can be subjective, but the scale of reconstructed value shows that when thresholded with the same level will produce information about the level of deposit.



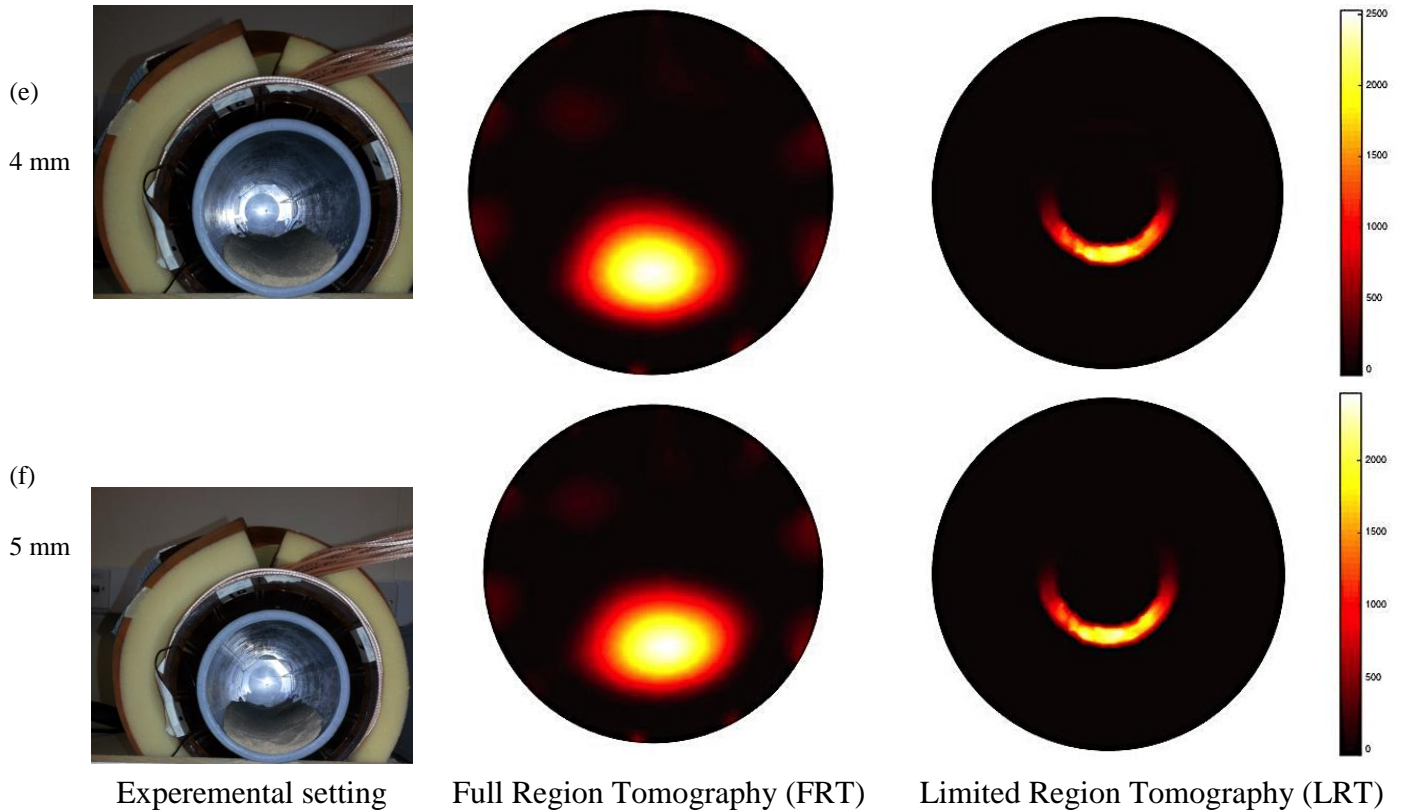


Fig. 8. Reconstruction of sand grains samples as models of black powder deposits with various layers of sand.

5 DISCUSSION

From Fig. 7 and 8, it can be noticed that both LRT and FRT were able to detect fine deposits and give information about their location. However, the LRT could remarkably detect a layer of deposits as small as 0.5 mm without noise and generally provides a more robust solution in all experimental scenarios presented here. Nevertheless, in such 2D ECT imaging, the deposits to be imaged must cover the entire length of the ECT sensor, whilst in real applications, the deposits may be smaller or non-uniform especially in the case of black powder flowing in gas pipelines. In such cases, the proposed method can be employed for 3D ECT, which can promise better real life solutions.

As mentioned earlier the limited region chosen in the LRT, shown in Fig. 3.a, has a relatively uniform sensitivity due to its concentric location. To illustrate the advantage of this orientation, a singular value decomposition (SVD) analysis of the Jacobian matrix for the LRT and FRT was carried out, normalized and then compared, as shown in Fig. 10. In order to visualize the superiority of this technique, a new limited region was created according to Fig. 9 where the region of interest is now a shifted circle to the right. According to the Picard condition, the number of singular values above the noise level of the measurements represents the amount of information that can be extracted from the inverse model. It can be seen from Fig. 10 that only 29 singular values for the circle orientation (Fig. 9) were above the noise level, while both the

LRT and FRT had 57 and 52 singular values above the noise level respectively.

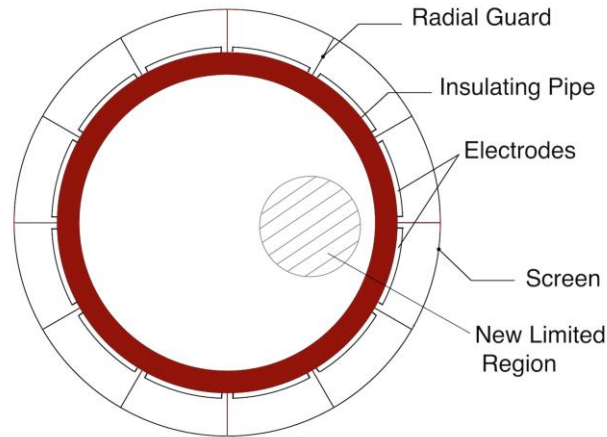


Fig. 9. New limited region, an example of a circle in the corner, created for the sake of comparison with the proposed LRT

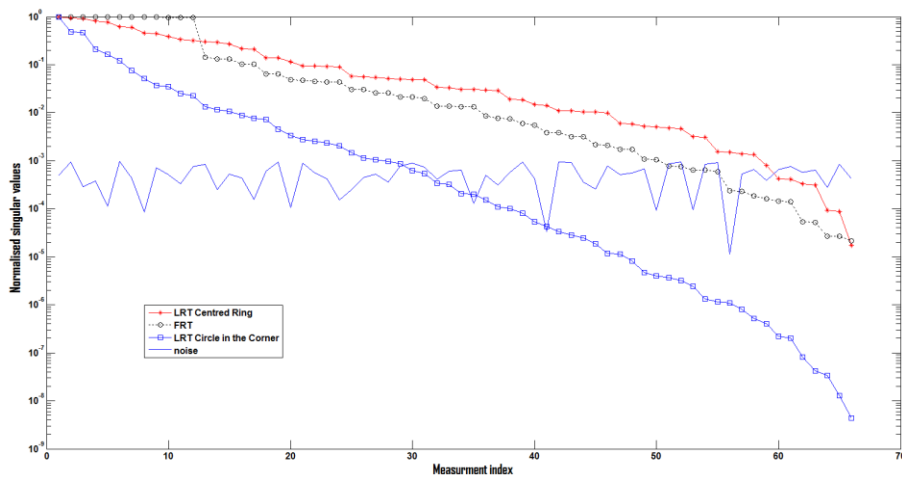


Fig. 10. Singular value decomposition (SVD) analysis of the Jacobian matrix for the LRT, FRT and new LRT

The experimental results in Fig. 7 show that different deposits regimes can be detected along the inner wall of the pipe. This conclusion is promising in terms of detecting deposits accumulation inside pipelines, which increases the interior pipe wall roughness and leads to other more serious problems. Also from Fig. 8, it can be seen that ECT can be used successfully to image accumulated grains as small as sand grains with 0.5 mm thickness of the deposited layer. This indicates that the proposed LRT method allows a detection of deposit with the resolution of 0.085 percent of the entire imaging region, which makes the ECT a very good method of detection of deposits.

Concluding from the results here, the ECT system with proposed LRT algorithm provides a non-invasive inspection method for plastic pipes. This inspection can help improve the accuracy of flowmeters; it can allow early detection and early removal of deposit which can be cost

effective. Further investigations are needed to develop methods that allow deposit detection in the presence of a flow inside of a pipe. ECT sensors can be designed in almost any geometrical forms, so proposed method could be extended to other geometries allowing inspection of deposit inside tanks and other types of vessels. It is envisaged that the LRT could provide superior resolution, but this has to be investigated in depth for a given situation.

6 CONCLUSION

In this study, a non-invasive and non-intrusive method for deposits and scales detection in pipelines was presented. The proposed method is based on ECT with limited region tomographic image reconstruction using a narrowband pass filter. Laboratory experiments were carried out using the suggested LRT and compared to the traditional FRT. The experimental results showed that different deposits regimes and small deposits as 0.5 mm could be detected. It is worth mentioning that the experiments conducted in this paper were static, which means no actual process flow was present in the test pipe, however, this method could be extended to detect deposits in the presence of a flow. Because of the promising results achieved in this study, further work will be carried out in order to develop an ECT deposit monitoring method with the presence of industrial flows of various phases. Also, the proposed method can be employed by other electrical tomography techniques for the detection of conductive deposits or deposits in metallic pipes, as ECT is only suitable for imaging the inside of dielectric materials non-invasively.

REFERENCES

- [1] M. Crabtree, D. Eslinger, P. Fletcher, M. Miller, A. Johnson and G. King, "Fighting Scale-Removal and Prevention," *Oilfield Review*, pp. 30-45, 1999.
- [2] L. Azevedo and A. Teixeira, "A critical review of the modelling of wax deposition mechanisms," *Petroleum Science and Technology*, Vol. 21, pp. 393-408, 2003.
- [3] Ararimeh Aiyejina, Dhurjati Prasad Chakrabarti, Angelus Pilgrim and M.K.S. Sastry, "Wax formation in oil pipelines: A critical review," *International Journal of Multiphase Flow*, vol. 37, Ino. 7, pp. 671-694, September 2011.
- [4] Richard M. Baldwin, "Black Powder problem will yield to understanding, planning," *Pipeline & Gas Industry*, pp. 109-112, 1999.
- [5] Olivier Trifilieff and Thomas H. Wines, "Black Powder Removal from Transmission Pipelines: Diagnostics and Solutions," Pall Corp., NY, USA, Rep. FCBLACKPEN, 2009.
- [6] M. S. Beck and R. A. Williams, "Process tomography: a European innovation and its applications," *Meas. Sci. Technol.*, vol 7, pp 215-224, 1996.
- [7] Zheng Liu and Yehuda Kleiner, "State of the art review of inspection technologies for condition assessment of water pipes," *Measurement*, vol. 46, no. 1, pp. 1-15, January 2013.

- [8] Zheng Liu and Yehuda Kleiner, "State-of-the-Art Review of Technologies for Pipe Structural Health Monitoring," *Sensors Journal, IEEE*, vol.12, no.6, pp.1987,1992, June 2012.
- [9] S.B. Costello, D.N. Chapman, C.D.F. Rogers N. Metje, "Underground asset location and condition assessment technologies," *Tunnelling and Underground Space Technology*, vol. 22, np. 5–6, pp. 524–542, September–November 2007.
- [10] Samir Abdul-Majid and Waleed AbulFaraj, "Asphalt and Paraffin Scale Deposit Measurement by Neutron Back Diffusion Using ^{252}Cf and $^{241}\text{Am-Be}$ Sources," in the 3rd Middle East Nondestructive Testing Conference & Exhibition (MENDT), Manama, Bahrain, 27-30 Nov 2005.
- [11] Alin Constantin Murariu, Aurel - Valentin Bîrdeanu, Radu Cojocaru, Voicu Ionel Safta, Dorin Dehelean, Lia Boțilă and Cristian Ciucă (2012). *Application of Thermography in Materials Science and Engineering, Infrared Thermography*, Dr. Raghu V Prakash (Ed.), ISBN: 978-953-51-0242-7, InTech, DOI: 10.5772/27507.
- [12] A. DeRosa, "Quenching the thirst of iron pipe," *Plastics News*, vol. 13, no. 32, pp. 1–3, 2001.
- [13] P.O. Moore (Ed.), *Nondestructive Testing Handbook: Ultrasonic Testing*, vol. 7. American Society for Nondestructive Testing Inc., Columbus, OH, USA, 2007.
- [14] W. Luo and J.L. Rose, "Guided wave thickness measurement with EMATs," *Insight*, vol. 45, no. 11, pp. 1–5, 2003.
- [15] Gongtian Shen and Gang Chen. "Infrared Thermography Test for High Temperature Pressure Pip," *Insight - Non-Destructive Testing and Condition Monitoring*, vol. 49, no. 3, pp. 151-153(3), March 2007.
- [16] S. M. Huang, A. Plaskowski, C. G. Xie and M. S. Beck, "Capacitance-based tomographic flow imaging system," *Electronics Letters*, Vol. 24, no, 7, pp 418–19, 1988.
- [17] K. Brodowicz, L. Maryniak and T. Dyakowski, "Application of capacitance tomography for pneumatic conveying processes," in *Proc. 1st ECAPT Conf. (European Concerted Action on Process Tomography)*, 1992, Manchester, March 26–29, 1992, ed. M S Beck, E Campogrande, M Morris, R A Williams and R C Waterfall (Southampton: Computational Mechanics) pp 361–8.
- [18] G. E. Fasching and N. S. Smith, "A capacitive system for three-dimensional imaging of fluidized beds," *Review of Scientific Instruments*, vol.62, no.9, pp.2243,2251, Sep 1991.
- [19] S.J. Wang, T. Dyakowski, C.G. Xie, R.A. Williams and M.S. Beck, "Real-time capacitance imaging of bubble formation at the distributor of a fluidized-bed," *Chem. Eng. J. Biochem. Eng.*, Vol. 56, no. 3, pp. 95–100, 1995.
- [20] S. Liu, W. Q. Yang, H. G. Wang and Y. Su, "Investigation of square fluidized beds using capacitance tomography: preliminary results" *Meas. Sci. Technol.* Vol. 12, no. 8, pp. 1120–5, 2001.
- [21] R. He, C. M. Beck, R. C. Waterfall and M. S. Beck, "Applying capacitance tomography to combustion phenomena," *Proc. 2nd ECAPT Conf. (European Concerted Action on Process Tomography)*, Karlsruhe, March 25–27, 1993 ed. M S Beck, E Campogrande, M Morris, R A Williams and R C Waterfall (Southampton: Comput Mechanics) pp 300–2.

- [22] R. He, C. M. Beck, R. C. Waterfall and M. S. Beck, "Finite element modelling and experimental study of combustion phenomena using capacitance measurements," Proc. 3rd ECAPT Conf. (European Concerted Action on Process Tomography), Porto, March 24–26, 1994, pp 367–76.
- [23] R. C. Waterfall, R. He, N. B. White and C. B. Beck, "Combustion imaging from electrical impedance measurements," *Meas. Sci. Technol.*, Vol. 7, pp. 369–74, 1996.
- [24] R. White, "Using electrical capacitance tomography to monitor gas voids in a packed bed of solids," *Measurement Science and Technology*, Vol. 13, no. 12, pp. 1842–1847, 2002.
- [25] Ø. Isaksen, A. S. Dico and E. A. Hammer, "A capacitance based tomography system for interface measurement in separation vessels," *Meas. Sci. Technol.*, Vol. 5, pp. 1262–71, 1994.
- [26] W. Q. Yang, M. S. Adam, R. Watson and M. S. Beck, "Monitoring water hammer by capacitance tomography," *Electron. Lett.*, Vol. 32, pp. 1778–9, 1996.
- [27] W. Deabes, and M. Abdelrahman, "Solution of the forward problem of electric capacitance tomography of conductive materials," in *The 13th World Multi- Conference on Systemics, Cybernetics and Informatics: WMSCI*, Orlando, Florida, USA, 2009.
- [28] W. Q. Yang and L. Peng, "Image reconstruction algorithms for electrical capacitance tomography," *Meas. Sci. Technol.*, vol. 14, no. 1, pp. R1–R13, Jan. 2003.
- [29] Ø. Isaksen, "A review of reconstruction techniques for capacitance tomography," *Meas. Sci. Technol.*, vol. 7, no. 3, pp. 325–337, Mar. 1996.
- [30] M. Soleimani and W. R. B. Lionheart, "Nonlinear image reconstruction for electrical capacitance tomography using experimental data," *Meas. Sci. Technol.*, vol. 16, pp. 1987–1996, 2005.
- [31] C.H. Mou, L.H. Peng, D.Y. Yao and D.Y. Xiao, "Image reconstruction using a genetic algorithm for electrical capacitance tomography," *Tsinghua Science and Technology*, vol.10, pp. 587–592, 2005.
- [32] M. Takei, "GVSPM image reconstruction for capacitance CT images of particles in a vertical pipe and comparison with the conventional method," *Measurement Science and Technology*, vol. 17, pp. 2104–2112, 2006.
- [33] C. Ortiz-Aleman, R. Martin and J.C. Gamio, "Reconstruction of permittivity images from capacitance tomography data by using very fast simulated annealing," *Measurement Science and Technology*, vol. 15, pp. 1382–1390, 2004.
- [34] Q. Marashdeh, W. Warsito, L.S Fan and F.L. Teixeira, "Non-linear image reconstruction technique for ECT using a combined neural network approach," *Measurement Science and Technology*, vol. 17, pp. 2097–2103, 2006.
- [35] W. Warsito and L.S. Fan, "Neural network based multi-criterion optimization image reconstruction technique for imaging two- and three-phase flow systems using electrical capacitance tomography," *Measurement Science and Technology*, vol. 12, pp. 2198–2210, 2001.
- [36] S. Liu, L. Fu, W.Q. Yang, H. Wang and F. Jiang, "Prior on-line iteration for image reconstruction with electrical capacitance tomography," *Science, Measurement and Technology*, vol.151, no. 3, pp. 195–

200, 2004.

[37] M. Soleimani, P. Yalavarthy and H. Dehghani, Helmholtz- "Helmholtz-Type Regularization Method for Permittivity Reconstruction Using Experimental Phantom Data of Electrical Capacitance Tomography," *Instrumentation and Measurement, IEEE Transactions on*, vol.59, no.1, pp.78,83, Jan. 2010.

[38] M. Soleimani, C.N. Mitchell, R. Banasiak, R. Wajman, A. Adler, "Four-dimensional electrical capacitance tomography imaging using experimental data," *Progress In Electromagnetics Research*, Vol. 90, pp.171-186, 2009.

[39] Jing Lei, Shi Liu, Xueyao Wang and Qibin Liu, "An image reconstruction algorithm for electrical capacitance tomography based on robust principle component analysis," *Sensors*, Vol.13, no. 2, pp.2076-92, 2013.

[40] Zhang Cao and Lijun Xu, "Direct image reconstruction for electrical capacitance tomography by using the enclosure method," *Meas. Sci. Technol.*, vol. 22, no. 10, 2011.

[41] Jing Lei, Shi Liu, Zhihong Li, Meng Sun and Xueyao Wang, "A multi-scale image reconstruction algorithm for electrical capacitance tomography," *Appl. Math. Modelling*, vol. 35, no. 6, pp 2585–606, 2011.

[42] D Watzenig, M Brandner and G Steiner, "A particle filter approach for tomographic imaging based on different state-space representations" *Meas. Sci. Technol.*, vol.18, pp. 30–40, 2007.

[43] Xinjie Wu, Guoxing Huang, Jingwen Wang and Chao Xu, "Image reconstruction method of electrical capacitance tomography based on compressed sensing principle," *Meas. Sci. Technol*, vol. 24, no, 7, 2013.

[44] B Kortschak, H Wegleiter and B Brandstätter, "Formulation of cost functionals for different measurement principles in nonlinear capacitance tomography," *Meas. Sci. Technol.* Vol. 18, no. 1, pp. 71–78, 2007.

[45] R. Banasiak and M. Soleimani, "Shape based reconstruction of experimental data in 3D electrical capacitance tomography," *NDT & E Int.* vol. 43, pp. 241–249 2010.

[46] Robert Banasiak, Radosław Wajman, Tomasz Jaworski, Paweł Fiderek, Henryk Fidos, Jacek Nowakowski and Dominik Sankowski, "Study on two-phase flow regime visualization and identification using 3D electrical capacitance tomography and fuzzy-logic classification," *International Journal of Multiphase Flow*, Vol.58, pp.1-14, 2014.

[47] W. A. Deabes, M. A. Abdelrahman, "A nonlinear fuzzy assisted image reconstruction algorithm for electrical capacitance tomography," *ISA Transactions*, Vol.49, no. 1, pp.10-18, 2010.

[48] M. Evangelidis, L. Ma, and M. Soleimani, "High definition electrical capacitance tomography for pipeline inspection," *Progress In Electromagnetics Research*, vol. 141, 2013.

[49] M. Zhang, E. Al Hosani, and M. Soleimani, "A limited region electrical capacitance tomography for detection of wax deposits and scales in pipelines," in the 5th International Workshop on Process Tomography (IWPT-5), Jeju, South Korea, September 16-18, 2014.